Implicit Transfer Operator Learning: Multiple Time-Resolution Surrogates for Molecular Dynamics

Mathias Schreiner*
DTU†
matschreiner@gmail.com

Ole Winther
DTU

Simon Olsson‡
Chalmers University of Technology
simonols@chalmers.se

Abstract

Computing properties of molecular systems rely on estimating expectations of the (unnormalized) Boltzmann distribution. Molecular dynamics (MD) is a broadly adopted technique to approximate such quantities. However, stable simulations rely on very small integration time-steps (10^{-15} s), whereas convergence of some moments, e.g. binding free energy or rates, might rely on sampling processes on time-scales as long as 10^{-1} s, and these simulations must be repeated for every molecular system independently. Here, we present Implict Transfer Operator (ITO) Learning, a framework to learn surrogates of the simulation process with multiple time-resolutions. We implement ITO with denoising diffusion probabilistic models with a new SE(3) equivariant architecture and show the resulting models can generate self-consistent stochastic dynamics across multiple time-scales, even when the system is only partially observed. Finally, we present a coarse-grained CG-SE3-ITO model which can quantitatively model all-atom molecular dynamics using only coarse molecular representations. As such, ITO provides an important step towards multiple time- and space-resolution acceleration of MD.

1 Introduction

Numerical simulation of stochastic differential equations (SDE) is critical in the sciences, including statistics, physics, chemistry, and biology applications [1]. Molecular dynamics (MD) simulations are an important example of such simulations [2]. These simulations prescribe a set of mechanistic rules governing the time evolution of a molecular system through numerical integration of, for example, the Langevin equation [3]. MD grants mechanistic insights into experimental observables. These observables are expectations, including time-correlations, of observable functions (e.g., pairwise distances or angles) computed for the Boltzmann distribution $\hat{\mu}(\mathbf{x}) \propto \exp[-\beta U(\mathbf{x})]$ corresponding to the *potential* $U(\cdot) : \Omega \to \mathbb{R}$ of a M-particle molecular system, $\mathbf{x} \in \Omega \subset \mathbb{R}^{3M}$ kept at the inverse temperature $\beta = 1/kT$. However, stable numerical integration relies on time steps, τ, which are strictly smaller than the fastest characteristic time-scales of the molecular system (10^{-15} s, e.g., bond vibrations), yet many molecular systems are characterized by processes on
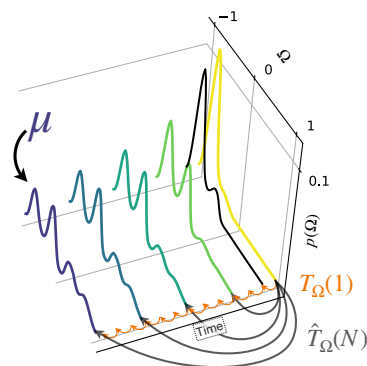

Figure 1: **Implicit Transfer Operator:** A multiple time-scale surrogate of stochastic molecular dynamics.

---

*Contributions to this work were done while visiting Chalmers University of Technology
†Technical University of Denmark
‡Corresponding author

much longer time-scales ($10^{-3} - 10^{-1}$ s, e.g. protein-folding, protein-ligand unbinding, regulation). Consequently, we need unfeasibly long simulations to characterize many important processes quantitatively due to the slow mixing in Ω.

In this work, we present the implicit Transfer Operator (ITO, Fig. 1) as an effective way to learn multiple time-step surrogate models of the stochastic generating distribution of MD. To our knowledge, this is the first surrogate modeling approach that allows for the simultaneous generation of stochastic dynamics at multiple different time resolutions. By adopting an SE(3)-equivariant generative model, we further demonstrate stable long-time-scale dynamics in increasingly difficult settings where an increasing number of degrees of freedom are marginalized. Our approach can be several orders of magnitude more efficient than direct MD simulations and can be made asymptotically unbiased if the generative model permits exact likelihood evaluation.

Our contributions are

1. the **Implicit Transfer Operator (ITO)** framework for learning generative models for multiple time resolution molecular dynamics simulations,

2. **ChiroPaiNN** an efficient SE(3) equivariant message passing neural network,

3. implementation of ITO using a denoising diffusion probabilistic model (DDPM) [4] with strong empirical results across resolutions: **SE(3)-equivariant ITO model (SE3-ITO)** gives stable long time-scale simulations and self-consistent dynamics across multiple time-scales for molecular benchmarks and **Coarse-grained SE3-ITO model (CG-SE3-ITO)** trained on large-scale protein folding data sets shows quantitative agreement with major dynamic and stationary observables of interest.

2 Background and Preliminaries

Notation Throughout this work, diffusion time, related to Diffusion Models (see Sec. 2), and physical time are represented using superscripts and subscripts, respectively.

Molecular dynamics and observables Molecular dynamics (MD) is a wide-spread simulation strategy in computational chemistry and physics. In this approach, the time-evolution of N particles configuration in Euclidean space $\mathbf{x} \in \Omega \subset \mathbb{R}^{3M}$, is modeled via a stochastic differential equation (SDE) with a drift term based on a potential energy model $U(\mathbf{x}) : \Omega \to \mathbb{R}$. An important aim of MD is to compute:

1. **Stationary observables:** $O_f = \mathbb{E}_\mu[f(\mathbf{x})]$
2. **Dynamic observables:** $O_{f(t)h(t+\Delta t)} = \mathbb{E}_{\mathbf{x}_t \sim \mu}[\mathbb{E}_{\mathbf{x}_{t+\Delta t} \sim p_\tau(\mathbf{x}_{t+\Delta t}|\mathbf{x}_t)}[f(\mathbf{x}_t)h(\mathbf{x}_{t+\Delta t})]]$

where μ is the normalized Gibbs measure, and $p_\tau(\mathbf{x}_{t+\Delta t} \mid \mathbf{x}_t)$ is a conditional probability density function encoding the time-discrete evolution of the molecular system $\mathbf{x}$, with time-step $\Delta t = N\tau$ as prescribed by a dynamic model, e.g. *Langevin dynamics* [3], integrated with time-step, τ. N is typically a large integer. The functions $f, h : \Omega \to \mathbb{R}$ are observable functions or '*forward models*' describing the microscopic observation process, e.g. computing a distance or an angle. The observables, $O_{f(t)}$, and $O_{f(t)h(t+\Delta t)}$, include binding affinities and binding rates of a drug to a protein, respectively. Conventionally, these observables are estimated from simulation trajectories using naive Monte Carlo estimators.

For illustrative purposes, we assume the temporal behavior of a state, $\mathbf{x}$, follows the Brownian dynamics SDE (Itô form)

$$d\mathbf{x}_t = -\nabla U(\mathbf{x}_t)\gamma^{-1}\, dt + \sqrt{2D}dW, \tag{1}$$

where $D = \gamma^{-1}\beta^{-1}$ is a diffusion constant, with friction γ and inverse-temperature β, and dW is a Wiener process. Using the Euler–Maruyama time-discretization, with time-step τ, simulating the SDE corresponds to simulating a Markov chain with the transition probability density

$$p(\mathbf{x}_{t+\tau} \mid \mathbf{x}_t, \tau) = \mathcal{N}(\mathbf{x}_{t+\tau}|\mathbf{x}_t - \tau\nabla U(\mathbf{x}_t)\gamma^{-1}, \tau\sqrt{2D}\mathbb{I}_{3M}) \tag{2}$$

where $\mathcal{N}$ specifies the multi-variate Normal distribution, and $\mathbb{I}_{3M}$ is the $3M$-dimensional identity matrix. If τ is sufficiently small to allow stable simulation, the *invariant measure*, of the Markov chain

(eq. 2), is the Boltzmann distribution (normalized Gibbs measure) corresponding to the potential energy model $U(\mathbf{x})$ at β. Consequently, by simulating a large number of steps we can draw samples from μ to compute stationary observables and compute dynamic observables by simulating $\Delta t = N\tau$ steps enough times with initial states distributed according to μ. Explicit simulation make such computations extremely costly, and consequently, there's much interest in speeding up the calculations of these quantities.

Transfer Operators   Let ρ specify an initial condition, a probability density function on Ω. We can define a Markov operator $T_\Omega : L^1(\Omega) \to L^1(\Omega)$ using a transition density (e.g., 2):

$$[T_\Omega \circ \rho](\mathbf{x}_{t+\tau}) \triangleq \frac{1}{\mu(\mathbf{x}_{t+\tau})} \int_{x_t} \mu(\mathbf{x}_t)\rho(\mathbf{x}_t)p(\mathbf{x}_{t+\tau} \mid \mathbf{x}_t)\mathrm{d}\mathbf{x}_t \tag{3}$$

which then describes the μ-weighed evolution of absolutely convergent probability density functions on Ω according to eq. 1, with time-step, τ. Such an operator is called the (Ruelle) Transfer Operator [5, 6]. We can express the operator using a spectral form

$$T_\Omega(\tau) = \sum_{i=0}^{\infty} \lambda_i(\tau)|\psi_i\rangle\langle\phi_i| \tag{4}$$

where only eigenvalues $\lambda_i(\tau) = \exp(-\tau\kappa_i)$ depend on the time-step, τ. κ_i are characteristic 'relaxation' rates associated the left and right eigenfunction pair, ϕ_i and ψ_i [7]. We can compute the operator with time-lag $N\tau$ via the Chapman-Kolmogorov equation (see Sec. A.1, for details)

$$T_\Omega(N\tau) = \sum_{i=0}^{\infty} \lambda_i(\tau)^N|\psi_i\rangle\langle\phi_i|. \tag{5}$$

Equivariant Message Passing Neural Networks   In this work, we are concerned with MD, where the time-evolution of a molecule is governed by a force field $\mathcal{F}(\cdot) \triangleq -\nabla U(\cdot)$ derived from a central potential $U(\cdot)$. While $U(\cdot)$ is *invariant* to group-actions of the Euclidean group in three dimensions (E(3)), its corresponding force field is E(3)-*equivariant*. We call a function, f '*invariant*' under a group-action g iif $f(\mathbf{x}) = f(S_g\mathbf{x})$ and '*equivariant*' iff $T_g f(\mathbf{x}) = f(S_g\mathbf{x})$, where S_g and T_g are linear representations of the group element g [8].

While the force field $\mathcal{F}(\cdot)$ is equivariant under E(3) group-actions, in practice, classical molecular dynamics simulations do not change parity during simulation, and consequently, our data generating distribution — molecular dynamics — is equivariant under actions of the special E(3) (SE(3)) group, also called the group of rigid body motions, which excludes reflections.

As we aim to distinguish mirror images of molecules, we extend PaiNN [9], an E(3)-equivariant message passing neural network (MPNN), making it SE(3) equivariant by breaking its symmetry with respect to parity. Briefly, PaiNN embeds a graph $G = (V, E)$, where nodes, V, exchange equivariant messages through edges within a local neighborhood defined as $\mathcal{N}(i) = \{j \mid \|r_{ij}\| \leq r_{\text{cutoff}}\}$, where r_{ij} is the distance between nodes denoted i and j, and r_{cutoff} is the maximal distance at which nodes are allowed to exchange messages. Messages are pooled and subsequently used to update node features, thereby enabling exchange of equivariant information. We achieve parity symmetry-breaking by constructing the equivariant messages in a manner that depends on cross-products between equivariant node features and direction vectors between interacting nodes. The cross-product is an axial vector (i.e., does not change sign under parity). Consequently, by combining these vectors with polar vectors (change sign under parity), the model can learn to distinguish chiral molecules. We refer to this modified PaiNN architecture as ChiroPaiNN (CPaiNN). Further details are in the Appendix D.

Diffusion Models   The diffusion model (DM) formalism is a powerful generative modeling framework that learns distributions by modeling a gradual denoising process [4, 10, 11]. In DMs, we pre-specify a *forward diffusion process* (noising process), which gradually transforms the data distribution $p(\mathbf{x}^0)$ to a simple prior distribution $p(\mathbf{x}^T)$, e.g., a standard Gaussian, through a time-inhomogenous Markov process, described by the following SDE (Itô form)

$$\mathrm{d}\mathbf{x}^t = f(\mathbf{x}^t, t)\,\mathrm{d}t + g(t)\,\mathrm{d}W. \tag{6}$$

where $0 < t < T$ is the *diffusion time*, f and g are chosen functions, and dW is a Wiener process. We can generate samples from the data distribution $p(\mathbf{x}^0)$ by sampling from $p(\mathbf{x}^T)$ and solving the *backward diffusion process* (denoising process)

$$d\mathbf{x}^t = \left[f(\mathbf{x}^t, t) - g^2(t) \nabla_{\mathbf{x}^t} \log p(\mathbf{x}^t \mid t) \right] dt + g(t) \, dW \tag{7}$$

by approximating the *score field* $\nabla_{\mathbf{x}^t} \log p(\mathbf{x}^t \mid t)$ — or equivalently a time-dependent Gaussian transition kernel [4] — with a deep neural network surrogate $\nabla_{\mathbf{x}^t} \log \hat{p}(\mathbf{x}^t \mid t, \boldsymbol{\theta})$. We can use the learned score field to define a neural ordinary differential equation (ODE) [12, 13], or probability flow ODE [14] — eq. 7 less the term $g(t) \, dW$ and scaling $g^2(t)$ by $1/2$ — which we can leverage for efficient sampling and sample likelihood evaluation.

Here, we are concerned with building equivariant probability density functions under SE(3) group actions. Consequently, we parameterize the DM using a learned Gaussian transition kernel of a time-inhomogenous diffusion process. By restricting the transition kernels $p(\mathbf{x}^{t+1} \mid \mathbf{x}^t)$ to be equivariant under SE(3) group-actions, the marginal of $\mathbf{x}^{t+1}$ is always invariant [15]. Combining the equivariant transition kernel with an invariant prior density [16] ensures the whole Markov process is invariant to SE(3) group actions. Consequently, combining an isotropic mean-free Gaussian as prior with ChiroPaiNN-parameterized transition kernels, we can construct an SE(3) equivariant diffusion model.
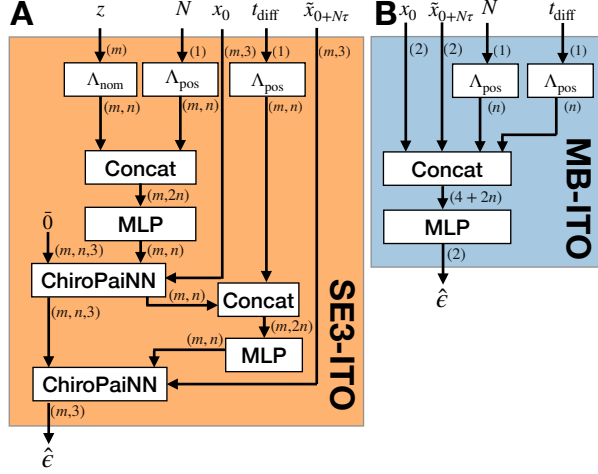

Figure 2: **ITO** $\hat{\epsilon}$ **networks** (A) SE3-ITO used for molecular application (B) MB-ITO, used for experiments with the Müller-Brown potential. Λ_{pos} and Λ_{nom} are positional and nominal embedding respectively, Concat is a concatenation, and MLP is a multi-layer perceptron. Arrows are annotated with input and output shapes.

3 Implicit Transfer Operator

We here consider simulation trajectories of a system as ancestral samples from a conditional probability density: $\mathbf{X} = \{\mathbf{x}_\tau, \ldots, \mathbf{x}_{N\tau}\} \sim p(\mathbf{x}_{n\tau} \mid \mathbf{x}_{(n-1)\tau})$, with $n = \{1, \ldots, N\}$, generated by explicit simulation by time-discretization of, for example, the Langevin equation. τ is a '*physical time-step*' determined by the integration scheme used to carry out MD. In general, the state variable $\mathbf{x}$, contains both position and velocity information of the particles, along with other details such as box dimensions, depending on the simulation scheme and target ensemble. Throughout this study, we only consider the position information.

If our MD simulation is performed with time-invariant potential energy (drift), we can express the generating transition probability as a decomposition of time-variant and -invariant parts (Proof, see Sec. A.2)

$$p(x_{N\tau} \mid x_0) = \sum_{i=1}^{\infty} \underbrace{\lambda_i^N(\tau)}_{\text{time-variant}} \underbrace{\alpha_i(x_{N\tau}) \beta_i(x_0)}_{\text{time-invariant}} \tag{8}$$

where α_i and β_i are *time-invariant* projection coefficients of the state variables on-to the left and right eigenfunctions ϕ_i and ψ_i, of the *Transfer operator* $T_\Omega(\tau)$ [5] and $|\lambda_i(\tau)| \leq 1$ is its i'th eigenvalue.

We build a surrogate of the conditional transition probability distribution (eq. 8) from MD data. In practice, we learn a generative model $\mathbf{x}_{t+N\tau} \sim p_{\boldsymbol{\theta}}(\mathbf{x}_{t+N\tau} \mid \mathbf{x}_t, N)$ with a conditional denoising diffusion probabilistic model (cDDPM) of the form

$$p(\mathbf{x}_{t+N\tau}^0 \mid \mathbf{x}_t, N) \triangleq \int p(\mathbf{x}_{t+N\tau}^{0:T} \mid \mathbf{x}_t, N) \, d\mathbf{x}^{1:T} \tag{9}$$

4

where $\mathbf{x}^{1:T}$ are *latent variables* of the same dimension as our output, and follow a joint density describing the backward diffusion process (eq. 7) and $\mathbf{x}^T \sim \mathcal{N}(0, \mathbb{1})$. We define a conditional sample likelihood as

$$\ell(\mathbf{I}; \theta) \triangleq \prod_{i \in \mathbf{I}} p_{\boldsymbol{\theta}}(\mathbf{x}_{t_i + N_i \tau}^0 \mid \mathbf{x}_{t_i}, N_i) \tag{10}$$

where $\mathbf{I}$ is a list of generated indices i specifying a time t_i and a time-lag (τ) integer multiple N_i, associating two time-points in the trajectory, $\mathbf{X}$. Following Ho et al., we train the cDDPM by optimizing a simplified form of the variational bound of the log-likelihood [4],

$$\mathcal{L}(\theta) = \mathbb{E}_{i \sim \mathbf{I}, \epsilon \sim \mathcal{N}(0, \mathbb{1}), t_{\text{diff}} \sim \mathcal{U}(0, T)} \left[\| \epsilon - \hat{\epsilon}_{\boldsymbol{\theta}}(\widetilde{\mathbf{x}}_{t_i + N_i \tau}^{t_{\text{diff}}}, \mathbf{x}_{t_i}, N_i, t_{\text{diff}}) \|_2 \right], \tag{11}$$

where $\widetilde{\mathbf{x}}_t^{t_{\text{diff}}} \triangleq \sqrt{\bar{\alpha}^{t_{\text{diff}}}} \mathbf{x}_t + \sqrt{1 - \bar{\alpha}^{t_{\text{diff}}}} \epsilon$, with $\bar{\alpha}^{t_{\text{diff}}} = \prod_i^{t_{\text{diff}}} (1 - \beta_i)$ and β_i is the variance of the forward diffusion process at diffusion time, i. $\hat{\epsilon}_{\boldsymbol{\theta}}(\cdot)$ is one of the two ITO neural network model architectures shown in Fig. 2, and is directly related to the score [4].

As outlined in Algorithm 1, we generate the indices $i \in \mathbf{I}$, in a manner such that the model is exposed to multiple time-lags, sampled uniformly across orders of magnitude, used for gradient-based optimization with Adam [17]. As a result, the model will be exposed to multiple different linear combinations of the eigenfunctions of $T_\Omega(\tau)$ in each batch during training. We conjecture that this data augmentation procedure will enable better learning of implicit representations of these eigenfunctions and, consequently, better generalization across time scales and yield more stable sampling.

3.1 ITO Architectures

We present two architectures for learning cDDPMs encoding ITO models, one for molecular applications SE3-ITO and one for the Müller-Brown benchmark system (Fig. 2). The SE3-ITO architecture uses our new SE(3) equivariant MPNN (ChiroPaiNN, described in sec. 2) to encode $\mathbf{x}_t$, N, and atom-types, z, to invariant features, s, and equivariant features, v. We concatenate s with an encoding of the diffusion-time t_{diff} and process them through a MLP (multi-layer perceptron). The output from the MLP are passed along with v and $\widetilde{\mathbf{x}}_t^{t_{\text{diff}}}$ as input to a second ChiroPaiNN module which predicts $\hat{\epsilon}$. More details on the architecture and hyperparameters are available in Appendices D and E.

Algorithm 1 Training. DisExp is defined in Appendix E

Input: n MD-trajectories; $\mathcal{X} = \{\mathbf{x}_0^j, \ldots, \mathbf{x}_{t_j}^j\}_{j=0}^n$, ITO score-model; $\hat{\epsilon}_{\boldsymbol{\theta}}$, max lag; $N_{\max}$
$\mathcal{X}' = \text{Concatenate}(\{\mathbf{x}_0^j, \ldots, \mathbf{x}_{t_j - N_{\max}}^j\}_{j=0}^n)$
while not converged **do**
 $\quad \mathbf{x}_t \sim \text{Choice}(\mathcal{X}')$
 $\quad N \sim \text{DisExp}(N_{\max})$
 $\quad t_{\text{diff}} \sim \text{Uniform}(0, T)$
 $\quad$ Take gradient step on:
 $\quad \nabla_{\boldsymbol{\theta}} \left[\| \epsilon - \hat{\epsilon}_{\boldsymbol{\theta}}(\widetilde{\mathbf{x}}_{t + N\tau}^{t_{\text{diff}}}, \mathbf{x}_t, N, t_{\text{diff}}) \|_2 \right]$
end while
return $\hat{\epsilon}_{\boldsymbol{\theta}}$

Algorithm 2 Ancestral sampling. Sampling from $p_{\boldsymbol{\theta}}$ is defined in Appendix E, Algorithm 4

Input: initial condition $\mathbf{x}_0$, lag N, nesting steps n.
Allocate $\mathcal{T} \in \mathbb{R}^{(n+1) \times \dim(\mathbf{x}_0)}$
$\mathcal{T}[0] = \mathbf{x}_0$
for $i = 1 \ldots n$ **do**
 $\quad \mathbf{x}_i \sim \hat{p}_{\boldsymbol{\theta}}(\mathcal{T}[i-1], N)$
 $\quad \mathcal{T}[i] = \mathbf{x}_i$
end for
return $\mathcal{T}$

---

4 Long time-step stochastic dynamics with Implicit Transfer Operators

4.1 Datasets and test-systems

To evaluate how robustly ITO models can model long time-scale dynamics, we conducted three classes of experiments, ranging from fully observed, high time-resolution, to sparsely observed and low time resolution. Details on training and computational resources are available in Appendices E and F, respectively.

Table 1: **VAMP2 score-gaps.** Difference in VAMP2-scores of ancestral sampling from ITO models with fixed lag and stochastic lags, compared to baseline Langevin simulations. Perfect match is 0, negative and negative values correspond to under and over estimation of meta-stability, respectively. Standard deviations on last decimal place are given in parentheses.

system \ lag	10	100
Müller-Brown (fixed)	-0.0351 (5)	-0.1189 (2)
Müller-Brown (stochastic)	**-0.0312** (4)	**-0.0970** (5)

Müller-Brown   is a 2D potential commonly used for benchmarking molecular dynamics sampling methods. We generate a training data-set by integrating eq. 1 with the Müller-Brown potential energy as $U(\mathbf{x})$ (For details, see Appendix B.1). This dataset corresponds to a fully observed case.

Alanine dipeptide   We use publicly available data from MDshare [18]. Simulation is performed with $2\,\text{fs}$ integration time-steps and data is saved at $1\,\text{ps}$ intervals. The simulations are performed in explicit solvation, but we only model the 22 atoms of the solute, without considering velocities. Consequently, this dataset is only partially observed.

Fast-folding proteins   We use molecular dynamics data previously reported by Lindorff-Larsen et al. on the fast-folding proteins Chignolin, Trp-Cage, BBA, and Villin [19]. The data is proprietary but available upon request for research purposes. The simulations were performed in explicit solvent with a $2.5\,\text{fs}$ time-step and the positions was saved at $200\,\text{ps}$ intervals. We coarse-grain the simulation by representing each amino-acid by the Euclidean coordinate of their $C\alpha$ atom as done previously [20], leading to 10, 20, 28, and 35 particles in each system respectively. Consequently, these data correspond to a mostly unobserved case.

4.2   Stochastic lag improves meta-stability prediction

In sec. 2, we conjecture that exposing an ITO model to multiple lag times during training leads to better and more robust models. To test this, we trained a set of models on the Müller-Brown dataset with fixed constant lags $N = \{10, 100, 1000\}$ (fixed lag) and a single model with $N \sim \text{DisExp}(1000)$ (stochastic lag) using the MB-ITO model (Fig. 2).

We find that the model trained with a stochastic lag systematically outperforms models trained with fixed lag (Table 1). We gauge the agreement by comparing Variational Approach to Markov Processes (VAMP)-2 scores [21] (for details, see Appendix G), between model samples and training data and find that both models tend to underestimate meta-stability compared to training data slightly. However, the model trained with stochastic lag is marginally closer to the reference values. We note that the difference in the ability of fixed and
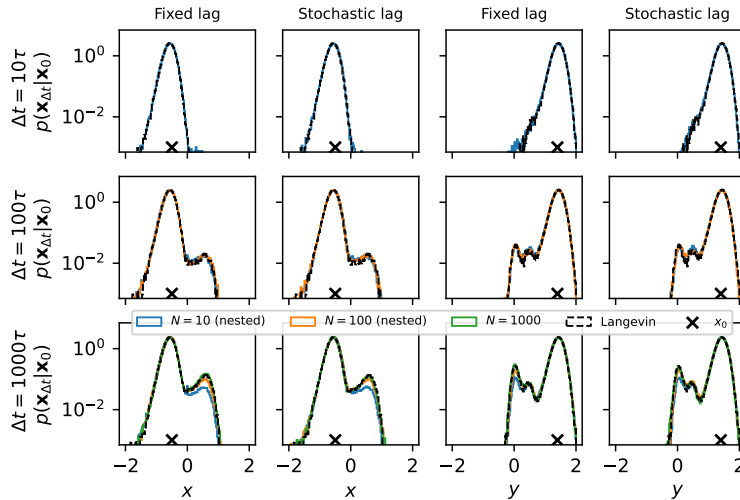

Figure 3: **Müller-Brown potential.** Conditional Probability Densities starting in x_0 indicated by cross, in ITO models trained with fixed or stochastic lag. Comparison of histograms of direct and ancestral sampling to direct simulation (Langevin). $N_{\text{samples}=250k}$

6

stochastic lag ITO models to capture long-time-scale dynamics is also reflected in the learned transition densities (Fig. 3). Together, these results suggest that lag-time augmentation during training leads to better implicit learning of the Transfer operator's eigenfunctions than training with a fixed lag.

4.3 Efficient and accurate self-consistent long time-scale dynamics

We evaluate the ITO models trained with stochastic lags to capture long time-scale dynamics in a self-consistent manner, in the Chapman-Kolmogorov sense, i.e., $p(\mathbf{x}_{\Delta t} \mid \mathbf{x}_0) \triangleq p(\mathbf{x}_{N\tau} \mid \mathbf{x}_0) = \prod_{i=1}^{N} p(\mathbf{x}_{i\tau} \mid \mathbf{x}_{(i-1)\tau})$, or if samples generated by direct sampling with time-step $\Delta t = N\tau$ are distributed similarly to samples generated by performing ancestral sampling N times, each with time-step τ.

For the fully-observed Müller-Brown case, we find that the ITO model is self-consistent by the strong overlap in transition densities sampled in a direct and ancestral manner (Algorithm 2). These results generalize to molecular systems and partially observed systems. Sampling an SE3-ITO model (Fig. 2) trained with alanine dipeptide data, we find strong agreement between the ancestrally and directly sampled transition densities (Fig. 4) and we again have a strong consistency with corresponding transition densities computed from molecular dynamics simulations. Note here, that the time-step of the ITO-sampled transition densities varies from 10^4 to 10^6 times the MD integration time-step.

Next, we consider four fast-folding proteins [19] where only the $C\alpha$ atoms are visible during model training. In this sparsely observed case (CG-SE3-ITO), we find strong model self-consistency, as shown by the comparison between conditional densities from the folded and unfolded states (Fig. 5) projected onto a linear subspace determined using *time-lagged independent component analysis* (time-lagged independent components, tIC) [22] (see Appendix B.3). Further, the long time-scale transition density gradually converges to the data distribution as expected.

Finally, by ancestral sampling (Algorithm 2), we perform a simulation of Chignolin with the same length as the training trajectory ($106\,\mu s$), using a CG-SE3-ITO model, and compare with MD. The CG-SE3-ITO simulation is 2120 steps with $\Delta t = 5\,\mathrm{ns}$. Running in parallel, on a single Titan X GPU we can simulate the CG-SE3-ITO model at a rate of $363\,\mathrm{ns}/(\mathrm{s}_w M^2)$ where s_w denotes seconds wall-time (Appendix C.2). Remarkably, these trajectories are virtually indistinguishable in the slowly

Figure 4: **Alanine dipeptide dynamics with SE3-ITO model**; Rows of increasing time-lag (from top to bottom). Contours are samples from SE3-ITO model, and 2D histograms show estimates from MD data. The first column shows conditional transition densities projected onto the torsion angles ϕ and ψ (inset). The black cross indicates the initial condition. The second and third columns show marginal distributions of ϕ and ψ, respectively, with direct sampling in orange, ancestral sampling in blue, and MD data in black.

relaxing TICA coordinates, illustrating stability of ITO. These conclusions extend to the proteins Villin, BBA, and Trp-Cage (See Appendix, Figs. 6,7 and 8)
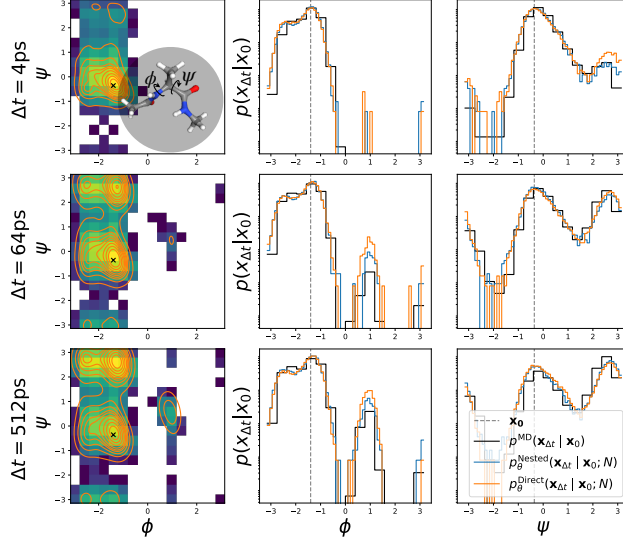
Together these results suggest that ITO models accurately and self-consistently capture the slow dynamics of molecular systems and are robust to situations where the system is only partially observed. In general, we expect robustness to sparsely observed representations as long as the input representations are sufficient to span the eigenfunctions of T_Ω [23, 24]. Approximation errors will translate into systematic under-estimation of relaxation time-scales [7], consistent with our slight
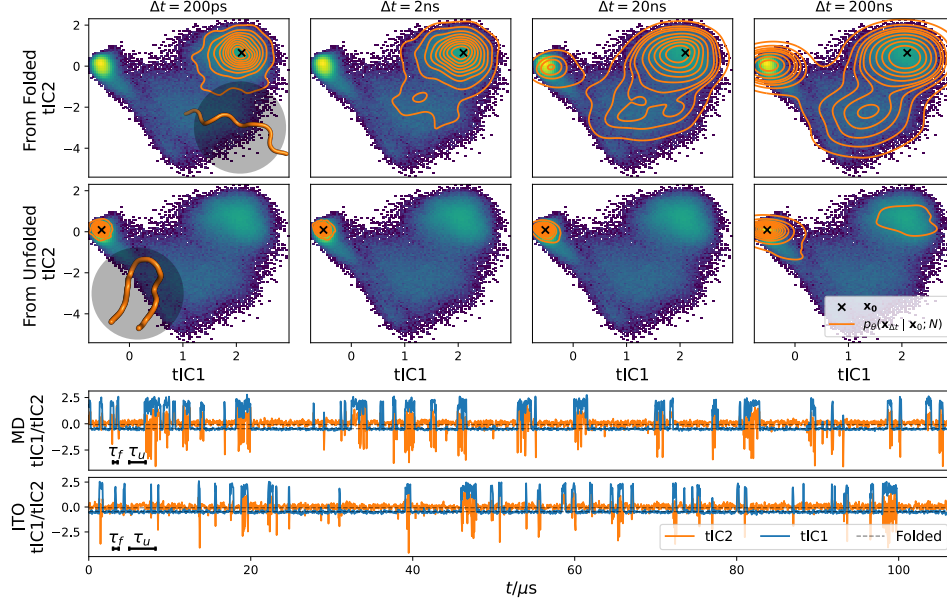
Figure 5: **Reversible protein folding-unfolding of Chignolin with CG-SE3-ITO** Conditional probability densities (orange contours) starting from folded (upper panels) and unfolded (lower panels) protein states, at increasing time-lag (left to right), shown on top of data distribution. Below: time-traces of 106 microsecond MD simulations and ITO simulations on tICs 1 and 2.

under-estimation of VAMP-2 scores (Table 1). In future work, combining the learning of SE3-ITO models with a systematic scheme for coarse-graining [25, 26], could be an avenue for scaling to large-scale molecular systems at a low computational cost.

5 Prediction of dynamic and stationary observables of using CG-SE3-ITO

As outlined in section 2, an important aim of MD simulations is to compute stationary and dynamic observables, which involves intractable integrals typically approximated via Monte Carlo estimators. Using the trained ITO models we can efficiently sample i.i.d. from the transition density needed for computing dynamic observables, and by choosing a time-step which is sufficiently large we can also sample i.i.d from the Boltzmann distribution μ, the latter akin to *Boltzmann generators* [27] (See Appendix A.1). We note that, the ITO models are surrogates and as such without reweighing we cannot expect unbiased samples from the Boltzmann and dynamic transition densities. Nevertheless, we gauge how accurately ITO models we can compute these observables of interest in the context of protein folding without reweighing:

- **Free Energy of Folding**, $\Delta G = -\log\left[\frac{p_f}{1-p_f}\right]$
- **Mean first passage time, folding**, $\langle\tau_f\rangle = \int_{x_0 \in \neg f} \int_0^\infty \delta(x_t \in f)p(x_t \mid x_0, t)t\,\mathrm{d}t\,\mathrm{d}x_0$
- **Mean first passage time, unfolding**, $\langle\tau_u\rangle = \int_{x_0 \in f} \int_0^\infty \delta(x_t \in \neg f)p(x_t \mid x_0, t)t\,\mathrm{d}t\,\mathrm{d}x_0$

where $\{f, \neg f\} \subset \Omega$ are disjoint subsets corresponding to the folded and unfolded states of a protein, $p_f = \int_{x \in f} \mu(x)\,\mathrm{d}x$, is the folded state probability and $\delta(\cdot)$ is the Dirac delta.

We compute these observables using the reference molecular simulation data [19] and samples statistics from the CG-SE3-ITO models of each of the four fast-folding proteins (details in Appendix C.1). Strikingly, the observables computed using CG-SE3-ITO models agree well with those computed from long all-atom MD simulations (Table 2).

We implemented all experiments using PyTorch[28], PyTorch Lightning[29], JAX[30], and used DPM-Solver[31] for probability flow ODE Sampling.

8

Table 2: **Molecular observables** Standard deviations on last decimal place are given in parentheses. Stationary and dynamic observables are denoted **s** and **d**, respectively.

	$\Delta G_{\text{fold}}/kT$ (**s**)	$\langle \tau_f \rangle / \mu s$ (**d**)	$\langle \tau_u \rangle / \mu s$ (**d**)
Chignolin (MD/ITO)	-1.28(1)/-1.53(2)	0.565(4)/0.700(8)	2.01(2)/3.24(4)
Trp-Cage (MD/ITO)	1.47(6)/2.84(6)	13.6(4)/37(2)	3.4(2)/2.85(9)
BBA (MD/ITO)	0.97(3)/1.52(3)	11.7(2)/8.6(2)	5.1(1)/1.75(4)
Villin (MD/ITO)	1.21(2)/2.22(3)	2.41(3)/3.27(7)	0.68(1)/0.354(5)

6 Related Work

Molecular sampling   Sampling molecular configurations is a broad field and can broadly be divided into two main areas: physically motivated sampling of the Boltzmann distribution and conformer generation. The first area includes algorithmic approaches to sample the Boltzmann distribution including Molecular Dynamics simulations [2], Markov Chain Monte Carlo, extended ensemble methods [32, 33, 34], including analysis methods involving deep generative nets [35], and surrogate models which directly approximate the Boltzmann distribution and allow for recovery of unbiased statistics, including Boltzmann generators [36, 16]. Conformer generation concerns generating physically plausible conformers without explicitly trying to follow the Boltzmann distribution. The latter approaches can be split into ML [15, 37, 38, 39, 40, 41, 42, 43, 44, 45, 46] and chemoinformatic [47, 48] approaches. Finally, speeding up molecular simulations by reducing the effective number of particles to simulate through coarse-graining with special purpose forcefield models [49] including machine learned variants [50, 51, 20, 52] and learned coarse-graining maps [25, 26] is an orthogonal approach to sample conformation space. Further, several methods to recover all-atom models from coarse-grained representations through ML [53, 54] and rule-based approaches [55] are available.

Transfer Operator surrogates   Building transfer operator surrogates is commonly used in molecular modeling including (Deep Generative) Markov state models (MSM) [56, 7, 57, 58], dynamic graphical models,[59] VAMPnets[60, 21], observable operator models[61], however, primarily for analysis of molecular dynamics data. Markov state models are time-space discrete approximations of the transfer operator and Deep Generative MSM [62] and VAMPnets [60] are deep learning infused versions, where state discretization is learned by deep nets. Dynamic graphical models reparameterize MSMs as kinetic Markov random fields allowing for scaling to larger systems [59]. Klein et al. recently introduced *timewarp* which is a flow-based generative model to simulate molecular systems with a large (up to $0.5\,\text{ns}$), fixed, time-lag, [63] providing asymptotically unbiased equilibrium samples through a Metropolis-Hastings correction [64]. While timewarp generates conformers with realistic local structure, it has limitations in capturing long time-scale dynamics, which is reflected in the predicted transition probability densities. In contrast, our approach captures long time-scale dynamics efficiently allowing for accurate prediction of dynamic observables.

7 Limitations

Surrogate model   Implicit Transfer Operators are surrogate models of stochastic dynamics' conditional transition probability densities. We cannot guarantee unbiased sampling of dynamics and the stationary distribution due to aleatoric (e.g., finite data) and epistemic (e.g., model misspecification) uncertainty. We can overcome the latter by reweighing against a Markov Chain Monte Carlo acceptance criterion as proposed previously [63], to ensure unbiased dynamics path-reweighing is necessary, which in turn requires closed-form expressions for the target path probabilities [65].

Transferability and scalability   Currently, ITO does not generalize across chemical space and thermodynamic variables. In future work, we anticipate that generalization across chemical space limitations can be overcome by appropriate data set curation and parameter-sharing schemes. Generalization across thermodynamic variables such as temperature and pressure would require using a surrogate model which is steerable under these changes, e.g., temperature steerable flows [66]. Currently, we assume a fully connected graph that scales $\mathcal{O}(M^2)$ in system size, which limits what systems are practically accessible. Devising new surrogate models which use mean-field approxima-

tion approaches from e.g., computational physics [67] or chemistry to truncate the graphs and treat long-range as an additive term [68] could yield more favorable scaling [69].

8 Conclusions

This paper introduces Implicit Transfer Operators (ITO), an approach to building multiple time-scale surrogate models of stochastic molecular dynamics. We implement ITO models with a conditional DDPM using a new time-augmentation scheme and show how ITO models capture fast and slow dynamics on benchmarks and molecular systems. We show ITO models are self-consistent over multiple time scales and highly robust to the marginalization of degrees of freedom in the system, which are unimportant to capture the long-time-scale dynamics. Combined with a new SE(3) equivariant MPNN architecture (ChiroPaiNN), we further show strong empirical evidence of scaling to applications, such as the folding of coarse-grained proteins. As such, we are confident that ITO is a stepping-stone toward general-purpose surrogates of molecular dynamics.

Acknowledgments and Disclosure of Funding

References

[1] Bernt Øksendal. *Stochastic Differential Equations*. Springer Berlin Heidelberg, 2003. DOI: 10.1007/978-3-642-14394-6. URL: https://doi.org/10.1007/978-3-642-14394-6.

[2] Daan Frenkel and Berend Smit. *Understanding Molecular Simulation*. Elsevier, 2002. DOI: 10.1016/b978-0-12-267351-1.x5000-7. URL: https://doi.org/10.1016/b978-0-12-267351-1.x5000-7.

[3] Paul Langevin. "Sur la théorie du mouvement brownien". In: *C. R. Acad. Sci. (Paris)* 146 (1908), 530—533.

[4] Jonathan Ho, Ajay Jain, and Pieter Abbeel. *Denoising Diffusion Probabilistic Models*. 2020. DOI: 10.48550/ARXIV.2006.11239. URL: https://arxiv.org/abs/2006.11239.

[5] David Ruelle. *Thermodynamic Formalism*. en. Encyclopedia of mathematics and its applications. Harlow, England: Longman Higher Education, Nov. 1978.

[6] Christof Schütte et al. "Conformation dynamics". In: *Proc. Int. Congr. ICIAM* (2009), pp. 297–336.

[7] Jan-Hendrik Prinz et al. "Markov models of molecular kinetics: Generation and validation". In: *The Journal of Chemical Physics* 134.17 (May 2011), p. 174105. DOI: 10.1063/1.3565032. URL: https://doi.org/10.1063/1.3565032.

[8] Jean-Pierre Serre. *Linear Representations of Finite Groups*. Springer New York, 1977. DOI: 10.1007/978-1-4684-9458-7. URL: https://doi.org/10.1007/978-1-4684-9458-7.

[9] Kristof T. Schütt, Oliver T. Unke, and Michael Gastegger. *Equivariant message passing for the prediction of tensorial properties and molecular spectra*. 2021. eprint: arXiv:2102.03150.

[10] Yang Song et al. *Score-Based Generative Modeling through Stochastic Differential Equations*. 2020. DOI: 10.48550/ARXIV.2011.13456. URL: https://arxiv.org/abs/2011.13456.

[11] Jascha Sohl-Dickstein et al. "Deep Unsupervised Learning using Nonequilibrium Thermodynamics". In: *Proceedings of the 32nd International Conference on Machine Learning*. Ed. by Francis Bach and David Blei. Vol. 37. Proceedings of Machine Learning Research. Lille, France: PMLR, 2015, pp. 2256–2265. URL: https://proceedings.mlr.press/v37/sohl-dickstein15.html.

[12] Ricky T. Q. Chen et al. "Neural Ordinary Differential Equations". In: *Advances in Neural Information Processing Systems*. Ed. by S. Bengio et al. Vol. 31. Curran Associates, Inc., 2018. URL: `https://proceedings.neurips.cc/paper_files/paper/2018/file/69386f6bb1dfed68692a24c8686939b9-Paper.pdf`.

[13] Will Grathwohl et al. "Scalable Reversible Generative Models with Free-form Continuous Dynamics". In: *International Conference on Learning Representations*. 2019. URL: `https://openreview.net/forum?id=rJxgknCcK7`.

[14] Yang Song et al. "Score-Based Generative Modeling through Stochastic Differential Equations". In: *International Conference on Learning Representations*. 2021. URL: `https://openreview.net/forum?id=PxTIG12RRHS`.

[15] Minkai Xu et al. *GeoDiff: a Geometric Diffusion Model for Molecular Conformation Generation*. 2022. eprint: `arXiv:2203.02923`.

[16] Jonas Köhler, Leon Klein, and Frank Noe. "Equivariant Flows: Exact Likelihood Generative Learning for Symmetric Densities". In: *Proceedings of the 37th International Conference on Machine Learning*. Ed. by Hal Daumé III and Aarti Singh. Vol. 119. Proceedings of Machine Learning Research. PMLR, 2020, pp. 5361–5370. URL: `https://proceedings.mlr.press/v119/kohler20a.html`.

[17] Diederik P. Kingma and Jimmy Ba. *Adam: A Method for Stochastic Optimization*. 2014. eprint: `arXiv:1412.6980`.

[18] URL: `https://markovmodel.github.io/mdshare/ALA2/#alanine-dipeptide`.

[19] K. Lindorff-Larsen et al. "How Fast-Folding Proteins Fold". In: *Science* 334.6055 (Oct. 2011), pp. 517–520. DOI: `10.1126/science.1208351`. URL: `https://doi.org/10.1126/science.1208351`.

[20] Marloes Arts et al. *Two for One: Diffusion Models and Force Fields for Coarse-Grained Molecular Dynamics*. 2023. eprint: `arXiv:2302.00600`.

[21] Hao Wu and Frank Noé. "Variational Approach for Learning Markov Processes from Time Series Data". In: *Journal of Nonlinear Science* 30.1 (2019), pp. 23–66. DOI: `10.1007/s00332-019-09567-y`. URL: `https://doi.org/10.1007%2Fs00332-019-09567-y`.

[22] Guillermo Pérez-Hernández et al. "Identification of slow molecular order parameters for Markov model construction". In: *The Journal of Chemical Physics* 139.1 (July 2013), p. 015102. DOI: `10.1063/1.4811489`. URL: `https://doi.org/10.1063/1.4811489`.

[23] Natasa Djurdjevac, Marco Sarich, and Christof Schütte. "Estimating the Eigenvalue Error of Markov State Models". In: *Multiscale Modeling & Simulation* 10.1 (Jan. 2012), pp. 61–81. DOI: `10.1137/100798910`. URL: `https://doi.org/10.1137/100798910`.

[24] Marco Sarich, Frank Noé, and Christof Schütte. "On the Approximation Quality of Markov State Models". In: *Multiscale Modeling & Simulation* 8.4 (Jan. 2010), pp. 1154–1177. DOI: `10.1137/090764049`. URL: `https://doi.org/10.1137/090764049`.

[25] Andreas Krämer et al. "Statistically Optimal Force Aggregation for Coarse-Graining Molecular Dynamics". In: *The Journal of Physical Chemistry Letters* 14.17 (Apr. 2023), pp. 3970–3979. DOI: `10.1021/acs.jpclett.3c00444`. URL: `https://doi.org/10.1021/acs.jpclett.3c00444`.

[26] Wangfei Yang et al. "Slicing and Dicing: Optimal Coarse-Grained Representation to Preserve Molecular Kinetics". In: *ACS Central Science* 9.2 (Jan. 2023), pp. 186–196. DOI: `10.1021/acscentsci.2c01200`. URL: `https://doi.org/10.1021/acscentsci.2c01200`.

[27] Frank Noé et al. "Constructing the equilibrium ensemble of folding pathways from short off-equilibrium simulations". In: *Proceedings of the National Academy of Sciences* 106.45 (Nov. 2009), pp. 19011–19016. DOI: `10.1073/pnas.0905466106`. URL: `https://doi.org/10.1073/pnas.0905466106`.

[28] Adam Paszke et al. "PyTorch: An Imperative Style, High-Performance Deep Learning Library". In: 32 (2019). Ed. by H Wallach et al. URL: `https://proceedings.neurips.cc/paper_files/paper/2019/file/bdbca288fee7f92f2bfa9f7012727740-Paper.pdf`.

[29] William Falcon and The PyTorch Lightning team. *PyTorch Lightning*. Version 1.4. Mar. 2019. DOI: `10.5281/zenodo.3828935`. URL: `https://github.com/Lightning-AI/lightning`.

[30] James Bradbury et al. *JAX: composable transformations of Python+NumPy programs*. Version 0.3.13. 2018. URL: `http://github.com/google/jax`.

[31] Cheng Lu et al. "DPM-Solver: A Fast ODE Solver for Diffusion Probabilistic Model Sampling in Around 10 Steps". In: *arXiv preprint arXiv:2206.00927* (2022).

[32] Jes Frellsen et al. "Bayesian Generalised Ensemble Markov Chain Monte Carlo". In: *Proceedings of the 19th International Conference on Artificial Intelligence and Statistics*. Ed. by Arthur Gretton and Christian C. Robert. Vol. 51. Proceedings of Machine Learning Research. Cadiz, Spain: PMLR, 2016, pp. 408–416. URL: http://proceedings.mlr.press/v51/frellsen16.html.

[33] Alessandro Laio and Michele Parrinello. "Escaping free-energy minima". In: *Proceedings of the National Academy of Sciences* 99.20 (2002), pp. 12562–12566. ISSN: 0027-8424. DOI: 10.1073/pnas.202427399. eprint: https://www.pnas.org/content/99/20/12562.full.pdf. URL: https://www.pnas.org/content/99/20/12562.

[34] D. P. Landau, Shan-Ho Tsai, and M. Exler. "A new approach to Monte Carlo simulations in statistical physics: Wang-Landau sampling". In: *American Journal of Physics* 72.10 (2004), pp. 1294–1302. DOI: 10.1119/1.1707017. eprint: https://doi.org/10.1119/1.1707017. URL: https://doi.org/10.1119/1.1707017.

[35] Yihang Wang, Lukas Herron, and Pratyush Tiwary. "From data to noise to data for mixing physics across temperatures with generative artificial intelligence". In: *Proceedings of the National Academy of Sciences* 119.32 (Aug. 2022). DOI: 10.1073/pnas.2203656119. URL: https://doi.org/10.1073/pnas.2203656119.

[36] Frank Noé et al. "Boltzmann generators: Sampling equilibrium states of many-body systems with deep learning". In: *Science* 365.6457 (Sept. 2019). DOI: 10.1126/science.aaw1147. URL: https://doi.org/10.1126/science.aaw1147.

[37] Bowen Jing et al. *Torsional Diffusion for Molecular Conformer Generation*. 2022. eprint: arXiv:2206.01729.

[38] Elman Mansimov et al. "Molecular geometry prediction using a deep generative graph neural network". In: *Scientific Reports* 9.1 (2019), pp. 1–13.

[39] Chence Shi et al. *Learning Gradient Fields for Molecular Conformation Generation*. 2021. eprint: arXiv:2105.03902. URL: http://arxiv.org/abs/2105.03902.

[40] Gregor Simm and Jose Miguel Hernandez-Lobato. "A Generative Model for Molecular Distance Geometry". In: *Proceedings of the 37th International Conference on Machine Learning*. Ed. by Hal Daumé III and Aarti Singh. Vol. 119. Proceedings of Machine Learning Research. PMLR, 2020, pp. 8949–8958. URL: http://proceedings.mlr.press/v119/simm20a.html.

[41] Chence Shi et al. "Learning Gradient Fields for Molecular Conformation Generation". In: *Proceedings of the 38th International Conference on Machine Learning*. Ed. by Marina Meila and Tong Zhang. Vol. 139. Proceedings of Machine Learning Research. PMLR, 2021, pp. 9558–9568. URL: https://proceedings.mlr.press/v139/shi21b.html.

[42] Tarun Gogineni et al. "TorsionNet: A Reinforcement Learning Approach to Sequential Conformer Search". In: *CoRR* abs/2006.07078 (2020). arXiv: 2006.07078. URL: https://arxiv.org/abs/2006.07078.

[43] Robin Winter, Frank Noé, and Djork-Arné Clevert. *Auto-Encoding Molecular Conformations*. 2021. URL: http://arxiv.org/abs/2101.01618.

[44] Victor Garcia Satorras et al. *E(n) Equivariant Normalizing Flows for Molecule Generation in 3D*. 2021. eprint: 2105.09016. URL: http://arxiv.org/abs/2105.09016.

[45] Niklas Gebauer, Michael Gastegger, and Kristof Schütt. "Symmetry-adapted generation of 3d point sets for the targeted discovery of molecules". In: *Advances in Neural Information Processing Systems*. Ed. by H. Wallach et al. Vol. 32. Curran Associates, Inc., 2019. URL: https://proceedings.neurips.cc/paper/2019/file/a4d8e2a7e0d0c102339f97716d2fdfb6-Paper.pdf.

[46] Minkai Xu et al. *An End-to-End Framework for Molecular Conformation Generation via Bilevel Programming*. 2021. eprint: arXiv:2105.07246.

[47] Sereina Riniker and Gregory A. Landrum. "Better Informed Distance Geometry: Using What We Know To Improve Conformation Generation". In: *Journal of Chemical Information and Modeling* 55.12 (Nov. 2015), pp. 2562–2574. DOI: 10.1021/acs.jcim.5b00654. URL: https://doi.org/10.1021/acs.jcim.5b00654.

[48] Paul C. D. Hawkins et al. "Conformer Generation with OMEGA: Algorithm and Validation Using High Quality Structures from the Protein Databank and Cambridge Structural Database". In: *Journal of Chemical Information and Modeling* 50.4 (Mar. 2010), pp. 572–584. DOI: 10.1021/ci100031x. URL: https://doi.org/10.1021/ci100031x.

[49] Paulo C. T. Souza et al. "Martini 3: a general purpose force field for coarse-grained molecular dynamics". In: *Nature Methods* 18.4 (Mar. 2021), pp. 382–388. DOI: 10.1038/s41592-021-01098-3. URL: https://doi.org/10.1038/s41592-021-01098-3.

[50] Jiang Wang et al. "Machine Learning of Coarse-Grained Molecular Dynamics Force Fields". In: *ACS Central Science* 5.5 (Apr. 2019), pp. 755–767. DOI: 10.1021/acscentsci.8b00913. URL: https://doi.org/10.1021/acscentsci.8b00913.

[51] Brooke E. Husic et al. "Coarse graining molecular dynamics with graph neural networks". In: *The Journal of Chemical Physics* 153.19 (Nov. 2020), p. 194101. DOI: 10.1063/5.0026133. URL: https://doi.org/10.1063/5.0026133.

[52] Jonas Köhler et al. "Flow-Matching: Efficient Coarse-Graining of Molecular Dynamics without Forces". In: *Journal of Chemical Theory and Computation* 19.3 (Jan. 2023), pp. 942–952. DOI: 10.1021/acs.jctc.3c00016. URL: https://doi.org/10.1021/acs.jctc.3c00016.

[53] Soojung Yang and Rafael Gómez-Bombarelli. *Chemically Transferable Generative Backmapping of Coarse-Grained Proteins*. 2023. eprint: arXiv:2303.01569.

[54] Yaxin An and Sanket A. Deshmukh. "Machine learning approach for accurate backmapping of coarse-grained models to all-atom models". In: *Chemical Communications* 56.65 (2020), pp. 9312–9315. DOI: 10.1039/d0cc02651d. URL: https://doi.org/10.1039/d0cc02651d.

[55] Leandro E. Lombardi, Marcelo A. Martí, and Luciana Capece. "CG2AA: backmapping protein coarse-grained structures". In: *Bioinformatics* 32.8 (Dec. 2015), pp. 1235–1237. DOI: 10.1093/bioinformatics/btv740. URL: https://doi.org/10.1093/bioinformatics/btv740.

[56] Christof Schütte et al. *A Hybrid Monte Carlo Method for Essential Molecular Dynamics*. eng. Tech. rep. SC-98-04. Takustr. 7, 14195 Berlin: ZIB, 1998.

[57] William C. Swope, Jed W. Pitera, and Frank Suits. "Describing Protein Folding Kinetics by Molecular Dynamics Simulations. 1. Theory". In: *The Journal of Physical Chemistry B* 108.21 (Apr. 2004), pp. 6571–6581. DOI: 10.1021/jp037421y. URL: https://doi.org/10.1021/jp037421y.

[58] Brooke E. Husic and Vijay S. Pande. "Markov State Models: From an Art to a Science". In: *Journal of the American Chemical Society* 140.7 (Feb. 2018), pp. 2386–2396. DOI: 10.1021/jacs.7b12191. URL: https://doi.org/10.1021/jacs.7b12191.

[59] Simon Olsson and Frank Noé. "Dynamic graphical models of molecular kinetics". In: *Proceedings of the National Academy of Sciences* 116.30 (July 2019), pp. 15001–15006. DOI: 10.1073/pnas.1901692116. URL: https://doi.org/10.1073/pnas.1901692116.

[60] Andreas Mardt et al. "VAMPnets for deep learning of molecular kinetics". In: *Nature Communications* 9.1 (2018). DOI: 10.1038/s41467-017-02388-1. URL: https://doi.org/10.1038%2Fs41467-017-02388-1.

[61] Hao Wu, Jan-Hendrik Prinz, and Frank Noé. "Projected metastable Markov processes and their estimation with observable operator models". In: *The Journal of Chemical Physics* 143.14 (Oct. 2015), p. 144101. DOI: 10.1063/1.4932406. URL: https://doi.org/10.1063/1.4932406.

[62] Hao Wu et al. *Deep Generative Markov State Models*. 2018. eprint: arXiv:1805.07601.

[63] Leon Klein et al. *Timewarp: Transferable Acceleration of Molecular Dynamics by Learning Time-Coarsened Dynamics*. 2023. eprint: arXiv:2302.01170.

[64] W. K. Hastings. "Monte Carlo sampling methods using Markov chains and their applications". In: *Biometrika* 57.1 (Apr. 1970), pp. 97–109. DOI: 10.1093/biomet/57.1.97. URL: https://doi.org/10.1093/biomet/57.1.97.

[65] S. Kieninger and B. G. Keller. "Path probability ratios for Langevin dynamics—Exact and approximate". In: *The Journal of Chemical Physics* 154.9 (Mar. 2021), p. 094102. DOI: 10.1063/5.0038408. URL: https://doi.org/10.1063/5.0038408.

[66] Manuel Dibak et al. "Temperature steerable flows and Boltzmann generators". In: *Physical Review Research* 4.4 (Oct. 2022). DOI: 10.1103/physrevresearch.4.l042005. URL: https://doi.org/10.1103/physrevresearch.4.l042005.

[67]   V Rokhlin. "Rapid solution of integral equations of classical potential theory". In: *Journal of Computational Physics* 60.2 (Sept. 1985), pp. 187–207. DOI: 10.1016/0021-9991(85) 90002-6. URL: https://doi.org/10.1016/0021-9991(85)90002-6.

[68]   P. P. Ewald. "Die Berechnung optischer und elektrostatischer Gitterpotentiale". In: *Annalen der Physik* 369.3 (1921), pp. 253–287. DOI: 10.1002/andp.19213690304. URL: https://doi.org/10.1002/andp.19213690304.

[69]   Arthur Kosmala et al. *Ewald-based Long-Range Message Passing for Molecular Graphs*. 2023. eprint: arXiv:2303.04791.

[70]   Benjamin Trendelkamp-Schroer et al. "Estimation and uncertainty of reversible Markov models". In: *The Journal of Chemical Physics* 143.17 (Nov. 2015), p. 174101. DOI: 10.1063/1.4934536. URL: https://doi.org/10.1063/1.4934536.

[71]   Susanna Röblitz and Marcus Weber. "Fuzzy spectral clustering by PCCA+ application to Markov state models and data classification". In: *Advances in Data Analysis and Classification* 7.2 (May 2013), pp. 147–179. DOI: 10.1007/s11634-013-0134-6. URL: https://doi.org/10.1007/s11634-013-0134-6.

[72]   Igor Mezić. "Spectral Properties of Dynamical Systems, Model Reduction and Decompositions". In: *Nonlinear Dynamics* 41.1-3 (2005), pp. 309–325. DOI: 10.1007/s11071-005-2824-x. URL: https://doi.org/10.1007%2Fs11071-005-2824-x.

[73]   Moritz Hoffmann et al. "Deeptime: a Python library for machine learning dynamical models from time series data". In: *Machine Learning: Science and Technology* 3.1 (2021), p. 015009. DOI: 10.1088/2632-2153/ac3de0. URL: https://doi.org/10.1088%2F2632-2153%2Fac3de0.

A Properties of the Transfer operator

A.1 Relaxation of T_Ω spectrum

In this section, we outline the 'relaxation' or 'decay' of the spectral components of T_Ω as a function of time-step, τ. We use that $\langle\phi_i|\psi_i\rangle_\mu = \int \phi_i(x)\psi_i(x)\,\mathrm{d}\mu(x) = 1$ if $i = j$ and 0 if $i \neq j$, e.g. the eigenfunctions are orthonormal under the μ-weighed inner-product. Since $T_\Omega(\tau)$ is Markov, composing $T_\Omega(\tau)$ with itself N times we get,

$$
\begin{aligned}
[T_\Omega(\tau)]^N &= T_\Omega(\tau) \circ \cdots \circ T_\Omega(\tau) & (12)\\
&= \sum_{i=0}^\infty \lambda_i(\tau)|\psi_i\rangle\langle\phi_i|\lambda_i(\tau)|\psi_i\rangle\langle\phi_i|\ldots\lambda_i(\tau)|\psi_i\rangle\langle\phi_i| & (13)\\
&= \sum_{i=0}^\infty \lambda_i(\tau)^N|\psi_i\rangle\langle\phi_i|\psi_i\rangle_\mu\langle\phi_i|\ldots|\psi_i\rangle\langle\phi_i| & (14)\\
&= \sum_{i=0}^\infty \lambda_i(\tau)^N|\psi_i\rangle\langle\phi_i| & (15)
\end{aligned}
$$

We assume the dynamics governed by T_Ω are

1. reversible $\lambda_i \in \mathbb{R}$

2. measure-preserving $0 \leq |\lambda_i| \leq 1$

3. ergodic, $\lambda_0 = 1$ and $|\lambda_{i>0}| < 1$

where we have sorted the eigenvalues eigenfunction pairs in descending order. Consequently, for $N \to \infty$ we have $T_\Omega(N\tau) \to |\mathbb{1}\rangle\langle\mu|$, where $\mathbb{1}$ is the constant function.

A.2 Decomposition of transition density

In this section, we detail the decomposition of the transition density, $p(\mathbf{x}_{N\tau} \mid \mathbf{x}_0)$.

Let ρ specify an initial condition, an absolutely convergent probability density function on Ω. We can define a Transfer operator T_Ω using a transition probability density [6]:

$$
[T_\Omega \circ \rho](\mathbf{x}_{N\tau}) \triangleq \frac{1}{\mu(\mathbf{x}_{N\tau})} \int_{\mathbf{x}_0} \mu(\mathbf{x}_0)\rho(\mathbf{x}_0)p(\mathbf{x}_{N\tau} \mid \mathbf{x}_0)\,\mathrm{d}\mathbf{x}_0, \qquad T_\Omega : L^1(\Omega) \to L^1(\Omega) \qquad (16)
$$

which then describes the μ-weighed evolution of densities on Ω according to MD discretized in time by a step-size of τ. μ is a normalized Gibbs measure, or the Boltzmann distribution.

Since we only consider MD with time-invariant drift, only the eigenvalues $\lambda_i(\tau)$ of $T_\Omega(\tau)$ depend on τ. We can express arbitrary transition probabilities through a bilinear form

$$
p(\mathbf{x}_{N\tau} \mid \mathbf{x}_0) = \langle\delta_{\mathbf{x}_{N\tau}}|T_\Omega^N(\tau)|\delta_{\mathbf{x}_0}\rangle = \sum_{i=1}^\infty \lambda_i^N(\tau)\langle\delta_{\mathbf{x}_{N\tau}}|\phi_i\rangle\langle\psi_i|\delta_{\mathbf{x}_0}\rangle = \sum_{i=1}^\infty \lambda_i^N(\tau)\alpha_i(\mathbf{x}_{N\tau})\beta_i(\mathbf{x}_0)
$$

(17)

where α_i and β_i are *time-invariant* projections coefficients of the state variables on-to the eigenfunctions ϕ_i and ψ_i, and $\delta_{\mathbf{x}}$ is the Dirac delta centered at $\mathbf{x}$. $T_\Omega^N(\tau)$ means $T_\Omega(\tau)$ acting N times (See A.1).

B Datasets

Throughout we train on all available data, as it is often sparse and difficult to split in an appropriate manner due to rare events e.g. folding and unfolding.

Table 3: Details about the Alanine dipeptide data (taken verbatim from mdshare)

Property	Value
Code	ACEMD
Forcefield	AMBER ff-99SB-ILDN
Integrator	Langevin
Integrator time step	2 fs
Simulation time	250 ns
Frame spacing	1 ps
Temperature	300 K
Volume	$(2.3222nm)^3$ periodic box
Solvation	651 TIP3P waters
Electrostatics	PME
PME real-space cutoff	0.9 nm
PME grid spacing	0.1 nm
PME updates	every two time steps
Constraints	all bonds between hydrogens and heavy atoms

B.1 Müller Brown

We generate the Müller Brown data set used for training by integrating the 2D potential energy model:

$$U(x,y) = \sum_{i=1}^{4} A_i \exp\left[a_i(x - \bar{x}_i)^2 + b_i(x - \bar{x}_i)(y - \bar{y}_i) + c_i(y - \bar{y}_i)^2 \right] \qquad (18)$$

using simulating overdamped Langevin or Brownian dynamics SDE, through a Euler-Mayurama time-discretization, and where

$$\begin{aligned}
A &= (-200, -100, -170, 15) \\
a &= (-1, -1, -6.5, 0.7) \\
b &= (0, 0, 11, 0.6) \\
c &= (-10, -10, -6.5, 0.7) \\
\bar{x} &= (1, 0, -0.5, -1) \\
\bar{y} &= (0, 0.5, 1.5, 1).
\end{aligned} \qquad (19)$$

We we generate 32 trajectories with random initial conditions in the ranges

$$\begin{aligned}
x &= [-1.5, 1.2] \\
y &= [-0.2, 2.0],
\end{aligned} \qquad (20)$$

and save every 10th step after a burn-in of 1000 steps. Each trajectory is simulated for 100000 steps.

A separate testing set was generated in an identical manner but with a different random seed. The values in Table. 1 are computed compared to this test set.

B.2 Alanine dipeptide

We use the data from MDShare (Table 3) which consists of three independent trajectories of 250 ns each.

Pre-processing The atomic coordinates are standardized before model training, each atom has a unique nominal embedding as atom type.

B.3 Fast folding proteins

The original data was obtained upon request from DE Shaw Research, and details about the simulations are available in the original publication [19]. All configurations were preprocessed by centering them at the origin. Furthermore, all configurations were scaled to ensure a standard deviation of one across the dataset.

Table 4: MSM hyperparameters. All models used 100 cluster centers, and clustered in the 5 first TICs.

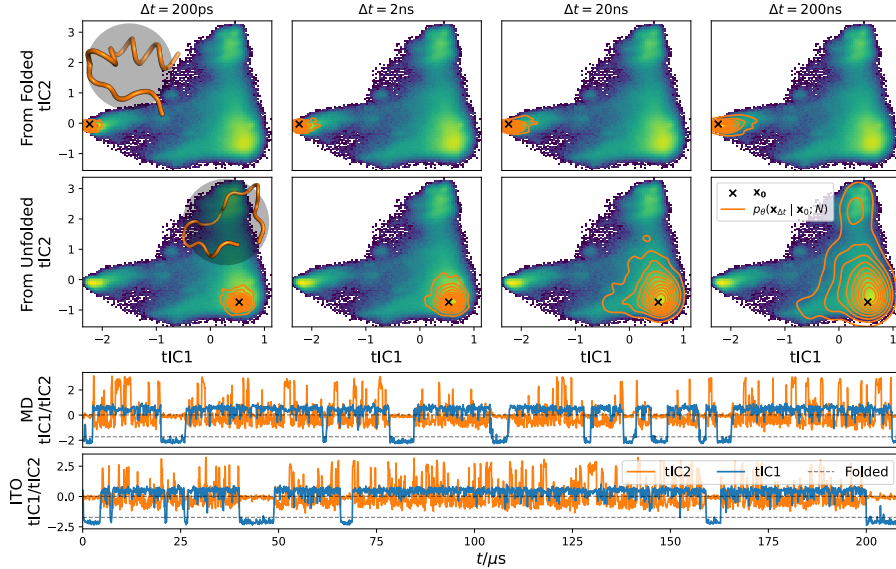|	TICA lag	MSM lag	ITO Δt
Chignolin	1ns	100ns	200ns
Trp-Cage	1ns	100ns	200ns
BBA	1ns	800ns	200ns
Villin	1ns	200ns	200ns

Figure 6: **Reversible protein folding-unfolding of Trp-Cage with CG-SE3-ITO** Conditional probability densities (orange contours) starting from folded (upper panels) and unfolded (lower panels) protein states, at increasing time-lag (left to right), shown on top of data distribution. Below: time-traces of 208 microsecond MD simulations and ITO simulations on tICs 1 and 2.

C   Additional results

C.1   Fast folding proteins

Figures 6, 7 and 8, show conditional distributions generated by CG-SE3-ITO models and comparisons of MD with ITO simulations on the fast folders Trp-Cage, BBA, and Villin, respectively.

Reference value and observables   We compute observables using Markov state models. First, we estimate a reference model for each system (see hyper-parameters in Table 4). Briefly, non-redundant and non-trivial pair-wise Cα distances were used as input for TICA dimension reduction, the reduced space was clustered using k-means. MSMs were sampled from a Bayesian posterior as previously described [70], using cluster assignments as state assignments. We identified folded and unfolded states using PCCA (Perron Cluster-Cluster analysis) [71], which in turn enabled the calculation of mean first passage times (MFPT) of folding $\langle \tau_f \rangle$ and unfolding $\langle \tau_u \rangle$ and the free energy of folding ΔG_{fold}.

Observables computed from ITO simulations were computed by processing the simulation data by projecting them onto the TICA space and the cluster centers determined on the MD data. MSMs were sampled as for MD data and observables were computed in the same way.

The reported uncertainties are standard deviations from Bayesian posterior sampling.
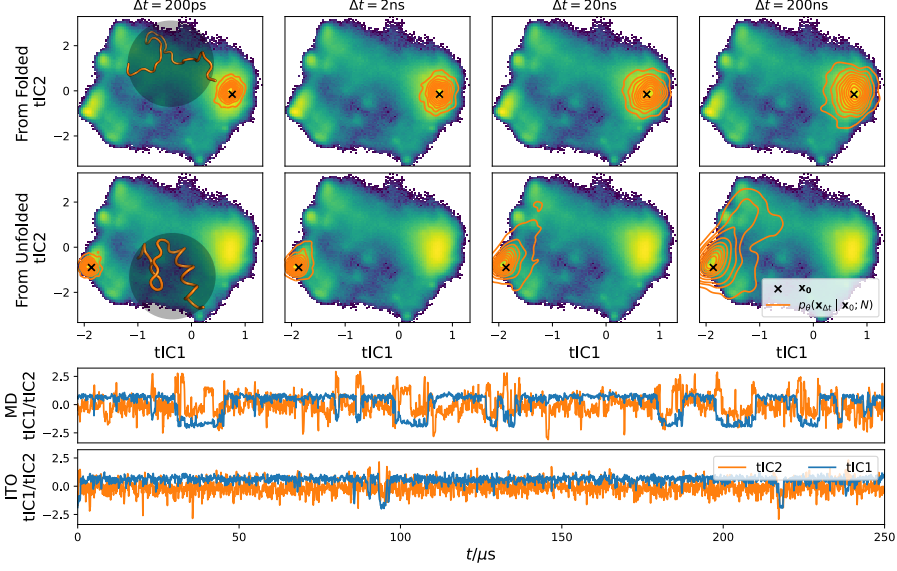
Figure 7: **Reversible protein folding-unfolding of BBA with CG-SE3-ITO** Conditional probability densities (orange contours) starting from folded (upper panels) and unfolded (lower panels) protein states, at increasing time-lag (left to right), shown on top of data distribution. Below: time-traces of 250 microsecond MD simulations and ITO simulations on tICs 1 and 2.

C.2 Sample timings

Running on a single device of a NVIDIA TITAN V node, using all memory, we can concurrently generate

- 253 simulation-steps/s for Chignolin
- 61 simulation-steps/s for Trp-Cage
- 35 simulation-steps/s for BBA
- 21 simulation-steps/s for Villin
- 48 simulation-steps/s for Alanine-Dipeptide

Note that all samples presented in this paper have been calculated equivalently using 50 ODE-steps. Depending on simulated lag, arbitrarily long trajectories can be sampled efficiently. Our models were trained on lags of up to 200 ns, but our findings suggest no constraints on extending the framework to much longer time scale.

D   Architectural details

Positional embedding, Λ_{pos}, maps diffusion time t_{diff}, physical time Δt, and interatomic distances r_{ij} to n-dimensional features-vectors with the n'th dimension defined as:

$$\Lambda_{\text{pos}}^n(x) = \begin{cases} \cos\left(\left(1 + \frac{n}{2}\right) x \frac{\pi}{l_0}\right) & \text{for even } n \\ \sin\left(\left(1 + \frac{n-1}{2}\right) x \frac{\pi}{l_0}\right) & \text{for odd } n, \end{cases} \tag{21}$$

where l_0 is a hyperparameter.

Nominal embedding Λ_{nom}, maps atomic elements or residue types to continuous n-dimensional feature vectors, $f : C \to R^n$, where C is the set of all categorical values and n is the dimension of the embedded vector.
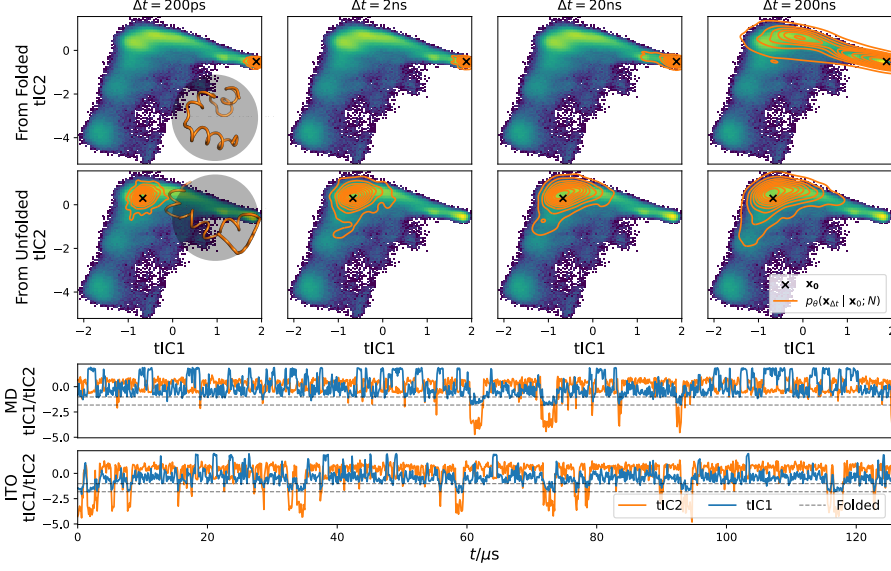
18

Figure 8: **Reversible protein folding-unfolding of Villin with CG-SE3-ITO** Conditional probability densities (orange contours) starting from folded (upper panels) and unfolded (lower panels) protein states, at increasing time-lag (left to right), shown on top of data distribution. Below: time-traces of 125 microsecond MD simulations and ITO simulations on tICs 1 and 2.
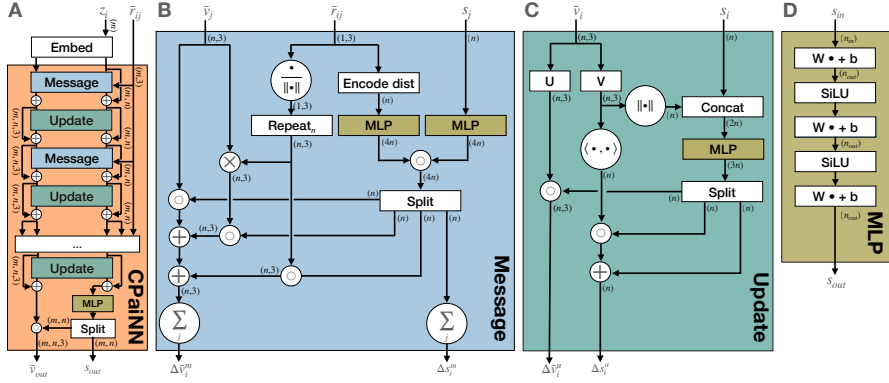

Figure 9: **ChiroPaiNN architecture** utilized in SE3-ITO and CG-SE3-ITO models (Fig. 2) for the embedding of conditional configuration and score prediction. Arrows are annotated with input and output shapes. $\times$ indicates cross product operations between all vectors along the first dimension, and $\circ$ indicates element-wise multiplication along the first dimension.

E   Training details

E.1   Sampling of configurations

The last $N_{\max}$ frames were truncated from each trajectory such that $\mathbf{x}_t$ could be sampled uniformly while keeping $\mathbf{x}_{t+N_{\max}}$ in bounds. N is sampled discretely from $\mathrm{DisExp}(N_{\max})$ following;

Algorithm 3 Sampling from DisExp

$N_{\log} \sim \mathrm{Uniform}(0, \log(N_{\max}))$
Return: $\mathrm{floor}(\exp(N_{\log}))$

Algorithm 4 Sampling from $\hat{p}_{\boldsymbol{\theta}}(\mathbf{x}_0, N)$

Input: initial condition $\mathbf{x}_0$, lag; N, diffusion steps; T_{diff}, ITO score-model; $\hat{\epsilon}_{\theta}$

$\mathbf{x}_N^{T_{\text{diff}}} \sim \mathcal{N}(\mathbf{0}, \mathbf{1})$

for $t_{\text{diff}} = T_{\text{diff}} \dots 1$ **do**

    $\epsilon \sim \mathcal{N}(\mathbf{0}, \mathbf{1})$

    $\mathbf{x}_N^{t_{\text{diff}}-1} = \frac{1}{\sqrt{\alpha^{t_{\text{diff}}}}} \left(\mathbf{x}_N^{t_{\text{diff}}} - \frac{1-\alpha^{t_{\text{diff}}}}{\sqrt{1-\bar{\alpha}^{t_{\text{diff}}}}} \hat{\epsilon}_{\theta}(\mathbf{x}_N^{t_{\text{diff}}}, \mathbf{x}_0, N, t_{\text{diff}}) \right) + \sigma_t \epsilon$

end for

return $\mathbf{x}_N^0$

E.2 Data splits

All available data was used for training with no test/validation set. Reference MFPT values are already coarse estimates and cannot be accurately calculated from a subset of the data due to slow time scales compared to the length of available trajectories.

E.3 Hyper Parameters

Müller-Brown   For the Müller-Brown results we trained with the MLP in MB-ITO architecture with 32 dimensional positional embeddings for t_{phys} and N and the MLP had 32 hidden nodes and 5 layers. We used a cosine learning rate scheduler and a sigmoidal β-scheduler with parameters as listed for alanine dipeptide and the fast folders. The model with stochastic lag was trained with $N_{\text{max}} = 1000$ and for fixed lag models N was fixed during data generation and the positional embeddings of N were removed from the model.

Alanine dipeptide and Fast folders   Hyperparameters employed for experiments on the fast folding proteins and Alanine Dipeptide are outlined below:

```
n_features: 64
n_message_passing_blocks_cpainn_embed: 2
n_message_passing_blocks_cpainn_score: 5

N_max: 1000
length_scale: 3.
beta_scheduler: sigmoidal(-8,-4)
diffusion_steps: 1000

batch_size: 128
learning_rate: 1e-3
optimizer: Adam
```

`n_message_passing_blocks_cpainn_{embed/score}` refers to the number of message passing and update blocks in the CPaiNN networks shown in Figure 2. A *message passing block* refers to a message block followed by an update block as shown in Figure 9. Where `sigmoidal(t_0,T)` $= \frac{1}{1+e^{-x}} \big|_{x \in (t_0, T)}$. `n_features` and `batch_size` corresponds to n and m in Figure 9. `length_scale` correspond to the value of l_0 in (Eq. 21) and defines the radial resolution of the embedding. `n_features` was chosen such that equivalent models could fit in memory of available hardware while maintaining a consistent `batch_size` across all systems. The remaining hyperparameters were fixed and were not systematically optimized.

E.4 Bond lengths Alanine Dipeptide

We evaluate how well the fast vibrational degrees of freedom are captured by the SE3-ITO model on Alanine dipeptide by inspecting the bondlength distributions of model samples (Fig. 10). The variances are generally over estimated slightly, but it does not appear to significantly our ability to predict slow dynamics. However, it would impact importance sampling as many configurations would have unfavorable physical energies. We leave it for future work to improve.
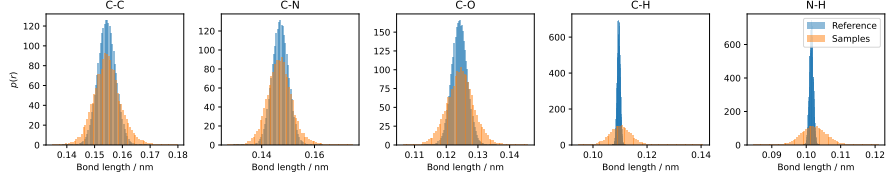
Figure 10: Bond lengths of samples Alanine Dipeptide

F   Compute resources

F.1   Training

All reported experiments have been conducted on NVIDIA TITAN V, NVIDIA TITAN X (Pascal), and NVIDIA GeForce GTX TITAN X's. All GPUs have ~ 12GB memory and range from 3000-5000 CUDA cores. Given the hyperparameters specified above, the SE3-ITO models converge within 2-4 days of training depending on system size.

Throughout the project, ~ 250 models were trained for an average duration of ~ 12 hours pr model on single GPU devices, resulting in a total of ~ 3000 GPU hours spent on training.

F.2   Sampling

In total 589 GPU hours have been spent on sampling throughout the entire project.

G   Variational Approach to Markov Processes (VAMP)

The Variational Approach to Markov Processes (VAMP) is a recent result in non-linear dynamics theory, its key contribution is a family of VAMP-scores [21]. The VAMP-scores are devised based upon the insight that the best (smallest prediction error) linear model can be expressed in terms of the top singular components of the Koopman operator, $\mathcal{K}$ [72]. The scores measure sum of the singular values of $\mathcal{K}$ multiplied by overlap coefficients between a set of (ortho-normalized) feature-maps f and g and the singular components of $\mathcal{K}$. We can optimize VAMP-scores to learn optimal feature mappings and Markovian models of the dynamics from time-series data [60] or for model comparison [21]. We here use the VAMP-score for the latter and assume $f = g$.

VAMP-r score is computed via the singular values of the Koopman matrix $\mathbf{K}$ estimated from data using the feature maps f and g [73],

$$\text{VAMP}-r = \sum_{i=0}^{k} \sigma_i^r \qquad (22)$$

where $r \in \mathbb{N}_+$.

G.1   VAMP gap

Informally, the VAMP-r scores quantify the meta-stability of a Koopman matrix. We define the VAMP-gap ΔV between two Koopman matrices, $\mathbf{K}$ and $\mathbf{K}'$, as the difference between their VAMP-2 scores:

$$\Delta V = \text{VAMP}-2(\mathbf{K}) - \text{VAMP}-2(\mathbf{K}'), \qquad (23)$$

where $\mathbf{K}'$ is a reference and $\mathbf{K}$ is a query matrix, respectively. In this context, $\Delta V = 0$ means meta-stability in $\mathbf{K}$ and $\mathbf{K}'$ is indistinguishable, $\Delta V < 0$ means $\mathbf{K}$ underestimates meta-stability, and *vice versa* for $\Delta V > 0$.